Simulation-Based Treatment Protocol Design for Damaging Breast Tumor Using Laser Photothermal Therapy

Edwin Quinn, Manpreet Singh, and Liang Zhu(✉)

University of Maryland Baltimore County, Baltimore, MD 21250, USA
zliang@umbc.edu

Abstract. Laser photothermal therapy utilizes gold nanorods/nanoshells embedded in tumors to enhance laser energy absorption in tumors via minimizing laser absorption in superficial tissue regions. The objective of this study is to develop a theoretical model to determine temperature elevations in a 10 mm diameter spherical tumor embedded inside a human breast model and to design a treatment protocol using laser photothermal therapy. Using the Pennes bioheat equation, we simulate temperature fields inside the tumor and its surrounding tissue before and during laser heating. Theoretical simulations show that using a laser intensity of 24000 W/m^2 at the skin surface with a laser spot of 10 mm in diameter, the maximal and minimal temperatures in the tumor are 65 °C and 47 °C, respectively. Equivalent minutes at 43 °C (EM_{43}) are used to assess accumulated thermal damage within the tissue during the heating. Results illustrate that the heating time for causing irreversible thermal damage to the entire tumor is 916 s using the selected laser intensity and spot size. Although cold-water droplets are sprayed at the skin surface to protect skin and its surrounding healthy tissue, it is found that collateral thermal damage to the healthy tissue near the tumor (up to 2 mm) is inevitable. We conclude that theoretical simulation is a useful tool to evaluate temperature field during laser photothermal therapy and to design effective and safe heating protocols in clinical applications.

Keywords: laser photothermal therapy · finite element simulation · bioheat transfer · breast cancer · heating protocol

1 Introduction

Recently, gold nanorods/nanoshells have been used to enhance laser absorption in tumors via a physical mechanism called Surface Plasmon Resonance [1–3]. Metallic (gold or silver) electrons resonantly oscillate and dissipate energy as heat, when the metal is subject to laser irradiation at a specific wavelength. The enhancement in laser energy absorption is several orders of magnitude higher than that of traditional dyes, such as indocynine green dye [4]. One could tune nanorods to have strong absorption and scattering to a specific laser wavelength by varying its geometrical parameters [5]. Nanorods/nanoshells can be directly injected into targeted tumors. The nanoparticles could stay inside the tissue for days or weeks before being cleared out, allowing multiple heating sessions to eradicate tumors.

W. Skalli et al. (Eds.): CMBBE 2023, LNCVB 39, pp. 96-104, 2024.
https://doi.org/10.1007/978-3-031-55315-8_11

Among a wide range of laser wavelengths, the near infrared (NIR) laser at ~800 nm is attractive to clinicians due to its deep optical penetration in normal tissue. Via selecting a near-infrared laser at ~800 nm in wavelength, one would expect minimal laser absorption in the superficial tissue region, and maximal laser energy absorbed by the gold nanorods embedded in the tumor. This would greatly confine laser energy in targeted tumor regions while minimizing collateral thermal damage to the surrounding healthy tissue. Previous experimental studies have demonstrated that gold nanorods were injected directly into tumors, and the absorption/scattering coefficients in nanorod-deposited tumors were almost twice of that in tumors without gold nanorods, leading to selective and enhanced laser energy absorption in those tumors [6, 7].

In this study, we simulate laser absorption in a tumor embedded in a human breast model to design heating treatment protocols. With previously extracted absorption/scattering properties in tissue with or without gold nanorod deposition [6], the Pennes bioheat equation [8] is used to simulate the temperature elevations in an embedded breast tumor during laser photothermal therapy. We then characterize the thermal damage inflicted on the breast tumor and to design a heating treatment protocol to maximally damage the entire tumor and minimize the collateral thermal damage to healthy tissue.

2 Methods

2.1 Geometry Overview

When laser photothermal therapy is used to damage an embedded tumor in the human breast, temperature elevations in the breast occur in the tissue region along the laser path and most of the laser energy is absorbed in the tumor due to embedded gold nanorods in the tumor. Although a human breast has a cone shape, in this study it is simplified as a cylindrical structure with an embedded spherical tumor, as shown in Fig. 1. This allows a short computational time without sacrificing accuracy of the simulated temperature elevations. A 10 mm diameter spherical tumor is embedded within the breast region, and its center is seated 10 mm from the skin surface. As shown in Fig. 1, the skin surface receiving laser irradiance is not curved, since the laser spot is significantly smaller than the curvature radius of a realistic breast at the skin surface. This allows simplification of the analyses of the laser induced source term distribution. The laser is incident across the projection of the tumor onto the skin, with a laser spot size of 10 mm in diameter. The temperature field is two-dimensional and axisymmetric.

As shown in Fig. 1, an 808 nm wavelength laser is assumed incident on the skin surface of the breast model and the laser then penetrates the healthy tissue before reaching the tumor. Due to the presence of nanorods in the tumor [6], significant laser absorption occurs in the tumor region. Based on the previous experimental results [6, 7], both the absorption coefficient and scattering coefficient in the normal breast tissue are much smaller than that in the tumor region with nanorod presence. In this study, the modified Beer's law is used to derive the volumetric heat generation rate distribution in both the tumor and surrounding healthy tissue regions. The modified Beer's law uses the irradiance at the tumor surface to model laser propagation along the laser path. In this study, it is assumed that the laser irradiance incident on the skin surface $I_{\lambda,0}$ (24000 W/m^2) is

uniform at the laser spot, and the spot size is selected as having the same diameter of the embedded tumor. The total laser power is 1.88 watts.

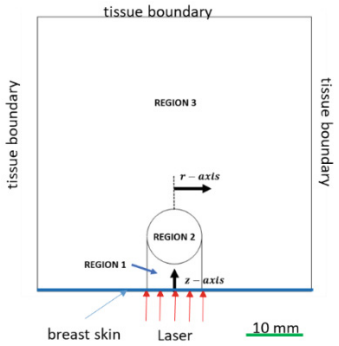

Fig. 1. Schematic diagram of the simplified model consisting of a tissue region with an embedded spherical breast tumor.

The entire simulation domain is divided into three regions. Region 1 represents the normal tissue region with laser absorption, and the volumetric heat generation rate distribution in Region 1 is derived as:

$$q'''_{Laser} = \mu_{eff,1} I_{\lambda,0} e^{-\mu_{eff,1} z} \tag{1}$$

where z represents the axial coordinate in the cylindrical coordinate system, and $\mu_{eff,1}$ is the attenuation coefficient related to the absorption coefficient (μ_a), the scattering coefficient (μ_s), and the anisotropic factor (g):

$$\mu_{eff,1} = \mu_{a,tissue} + (1-g)\mu_{s,tissue} \tag{2}$$

The anisotropic factor g in the above equation represents how uniform the scattering is in all the directions. For biological tissue, g usually is equal to 0.9–0.97, meaning most photons penetrate the tissue without scattering to superficial layers. In this study, we choose the value of g as 0.9, the same as that used in a previous study [9].

A similar attenuation coefficient in the tumor (Region 2) is defined as:

$$\mu_{eff,2} = \mu_{a,tumor} + (1-g)\mu_{s,tumor} \tag{3}$$

where the absorption and scattering coefficients in the tumor region are much bigger than that in the normal tissue region due to nanorod presence. The volumetric heat generation rate in Region 2 is a function of the radial and axial coordinates and is derived as follows:

$$q'''_{laser} = \mu_{eff,2} \cdot I_{\lambda,0} \cdot e^{-\mu_{eff,1}\left(z_o + r_o - \sqrt{r_o^2 - r^2}\right)} e^{-\mu_{eff,2}\left(z - z_o - r_o + \sqrt{r_o^2 - r^2}\right)} \tag{4}$$

where r_0 is the radius of the tumor and r is the radial coordinate in the cylindrical coordinate system. In theory, the tissue close to the tumor in Region 3 may still have some laser absorption even after the strong laser absorption enhancement in the tumor region. We assume that the laser absorption in Region 3 is negligible for simplification.

2.2 Temperature Field Simulation

The Pennes bioheat equation [8] is a modification from the traditional heat conduction equation with additional heat source and sink terms describing thermal contribution from metabolism and blood circulation in tissue:

$$\rho c \frac{\partial T}{\partial t} = k\nabla^2 T + \omega \rho_b c_b (T_b - T) + Q_{met} + q'''_{Laser} \tag{5}$$

where T is tumor/tissue temperature to be determined, subscript b denotes blood, T_b is the temperature of the arterial blood and is equal to 37 °C, k is thermal conductivity, ρ is density, Q_{met} is the metabolic heat generation rate, c is specific heat, and ω is the blood perfusion rate. $\boldsymbol{q'''_{Laser}}$ represents the volumetric heat generation rate in tissue/tumor induced by the laser incident on the skin.

At the skin surface with the laser irradiance, it is a convection boundary with a prescribed heat transfer coefficient h exposed to an ambient environment of T_∞, as:

$$-k\partial T/\partial n = h \cdot (T - T_\infty) \tag{6}$$

Before the laser treatment, the convection at the surface is due to free convection and radiation and the h value (h_1) is 15 W/m^{2}K and air temperature (T_∞) is 25 °C. During the laser treatment, to minimize thermal damage at the skin surface, cold water is typically sprayed at the skin surface within the laser spot. In this study, we assume that the convection coefficient (h_2) value is 1000 W/m^{2}K and the water droplet temperature ($T_{\infty,c}$) is 5 °C. The large h_2 value selected would result in a skin temperature closer to 5 °C during heating, shown later in the result section. The boundary condition at the other edges of the model are prescribed as 37 °C, with the assumption that those boundary surfaces are far away from the laser heating regions. The remainder of the skin surface that is not under laser irradiation experiences free convection.

Simulation of the temperature field is carried out by the finite element method in commercial COMSOL software. The simulation uses free triangular elements with the total number of elements as 36958 in the simulation domain. The mesh size and time step are decreased in all regions until less than 0.1% variations in the values of the maximal and minimal tumor temperatures are obtained.

2.3 Heating Protocol Design Using Thermal Damage Model

The temperature elevation history can be used to assess thermal damage in the tumor. If irreversible thermal damage is achieved at the lowest tumor temperature elevation location, one can conclude that irreversible thermal damage occurs in the rest of the tumor. Thermal dosage leading to irreversible thermal damage is assessed using the equivalent minute at 43 °C (EM_{43}) [10]. In early thermal damage experiments, a tissue sample was immersed into a water bath at 43 °C to determine how long it took to cause irreversible thermal damage. This measured heating time duration is called $EM_{43,critical}$, carrying a unit of minutes. The selected $EM_{43,critical}$ is 120 min based on previously measured experimental results. In other words, if the tissue sample were immersed into a water bath at 43 °C, it would have taken 120 min to completely damage the tissue.

However, in most hyperthermia treatments, temperature elevations at any tissue location are gradual, and its temperature may be lower or higher than 43 °C during the heating. It is necessary to determine the EM_{43} minutes during a realistic heating process. The following formula is used to calculate the value of the EM_{43} for any tissue locations at any time instants as following [10]:

$$\text{EM}_{43} \text{ for location } i = \sum_{j=1}^{n} \Delta t_j R^{43-T_i(t_j)}; R = \begin{cases} 0.25 & 37\,^{\circ}\text{C} \le T \le 43\,^{\circ}\text{C} \\ 0.50 & 43\,^{\circ}\text{C} \le T \le 48\,^{\circ}\text{C} \\ 0.72 & 48\,^{\circ}\text{C} \le T \end{cases} \quad (7)$$

Shown in Eq. 7, the heating duration is divided into individual segments (a total of n segments) with each time segment as Δt_j, during which the temperature at location i is assumed to be maintained as a constant as $T_i(t_j)$. R is called the R-value representing a modification to calculate the equivalent minutes at 43 °C from the actual heating duration, Δt_j. It has been demonstrated that the R-value also depends on the temperature range. In this study, we adopt the R-values from a previous study [10]. Equation 7 implies that the accumulative EM_{43} minutes is zero at the beginning of a heating duration, however, it increases with the heating, and the equivalent EM_{43} minutes would accelerate in later time when the temperature is much higher. In this study, based on the obtained temperature elevation history at the lowest temperature location of the tumor, the accumulative EM_{43} is calculated as a function of the heating time. The heating time instant when the EM_{43} reaches 120 min is then determined as the required heating duration to achieve irreversible thermal damage to the entire tumor.

3 Results

Thermal properties used in the simulation are listed in Table 1 [6, 9–11]. The volumetric laser absorption rate q'''_{Laser} in the normal tissue between the skin and the tumor (Region 1) is illustrated by the yellow and green contours in Fig. 2. Region 1 shows a decay of laser energy absorption from the superficial skin surface to the deep tissue region, depending only on the axial distance along the laser path z. Once the laser propagates into the tumor region (Region 2), the enhanced laser energy absorption due to the presence of nanorods is evident, illustrated by the dark red contours. At the far end of the tumor, the laser absorption is almost negligible.

The steady state temperature field prior to laser treatment is used as the initial condition of the transient temperature simulation. Figure 3 shows the temperature contours at the central slice of the simulation domain at various temperature instants. Once the laser treatment is initiated, one can see steady temperature elevations in the tissue region with laser absorption. The maximal temperature in the tumor region does not occur at the same location with the maximal q'''_{Laser}, rather it occurs at a deep tumor location, approximately 3 mm away from that tumor-tissue interface. Shown in Fig. 3, the tumor location with the maximal temperature rises from the initial 37 °C to 45 °C after 30 s, to 55 °C after 100 s, and finally, to 60 °C after 200 s. The steady state is established after heating for 362 s with a maximal tumor temperature of 65 °C. The minimal temperature of 47 °C after steady state occurs at the tumor far away from the skin surface. During

the heating, one notices significant temperature reductions (~10 °C) at the skin surface with the sprayed water droplets. Limited cooling penetration from the skin surface to deep tissue is observed.

Table 1. Thermal properties used in the simulation [6, 9–11]

Property	Value	Property	Value
ω_{Tumor}	0.00083 (1/s)	ω_{Tissue}	0.0033 (1/s)
$\mu_{eff,1}$	90 (1/m)	$\mu_{eff,2}$	180 (1/m)
c_{Tumor}	3500 (J/kg K)	c_{Tissue}	3950 (J/kg K)
$Q_{met,Tumor}$	2083 (W/m^3)	$Q_{met,Tissue}$	8332 (W/m^3)
k_{Tumor}	0.48 (W/m K)	k_{Tissue}	0.48 (W/m K)
cb	3800 (J/kg K)	ρ_b	1000 (kg/m^3)
T_∞	25 (°C)	$T_{\infty,c}$	5 (°C)
$h1$	15 (W/m^2 K)	h_2	1000 (W/m^2 K)
$I_{\lambda,0}$	24000 (W/m^2)	$EM_{43,critical}$	120 (Minutes)

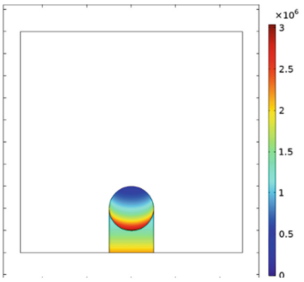

Fig. 2. Laser induced energy absorption rate distribution in the three tissue regions.

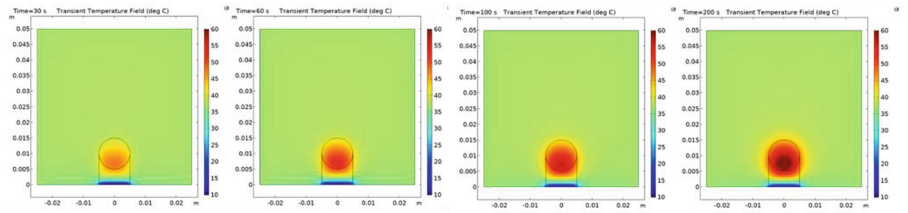

Fig. 3. Temperature fields in the tumor and its surrounding tissue are shown at time instants of 30 s, 60 s, 100 s, and 200 s, respectively.

The transient temperature elevation history is used to determine the required heating time to achieve 120 min of EM_{43} at the lowest temperature location in the tumor. Figure 4

illustrates the non-linear nature of the accumulation of the EM_{43} at the lowest temperature location in the tumor ($r = 0$ and $z = 0.015$ m), calculated using Eq. 7. EM_{43} at this location starts from zero before the heating and then increases slowly at the beginning of the heating duration. There are much faster increases in the EM_{43} in the later heating time, when the temperatures are much higher. Based on the curve shown in the left panel of Fig. 4, it takes 916 s for the EM_{43} at this location to reach the $EM_{43,\,critical}$ of 120 min. The right panel of Fig. 4 shows the EM_{43} accumulations of tissue locations along the central laser path at several time instances. After 916 s of heating the tumor location with the lowest temperature (i.e., at $r = 0$ m, $z = 0.015$ m) has an accumulative EM_{43} equal to 120 min. However, the collateral thermal damage also occurs in the normal tissue region near the tumor, up to 2.4 mm from the tissue-tumor interface.

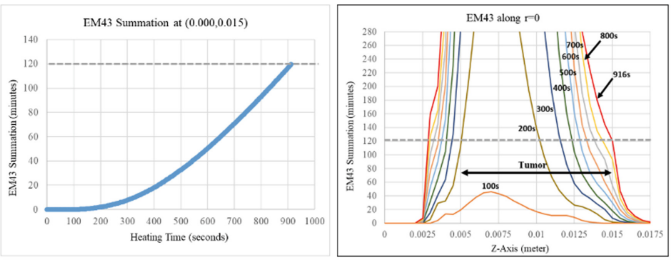

Fig. 4. Left panel: EM_{43} accumulation with time at the tumor location with the minimal temperature increase within the tumor. Right panel: EM_{43} distribution along laser path at the central line at various time instants.

4 Discussion

This study is meant to be a baseline analysis of the viability of the approach for treating deeply seated breast tumors. The research is based on experimentally extracted laser radiation properties in a previous *in vivo* experiment [9]. The obtained temperature fields before and during laser photothermal therapy are similar to previous experimental results. The required laser power of approximately 1.88 W and the laser heating duration are in good agreement with previous experimental results that show tumor shrinkage after treatment. Future experimental measurements of temperature elevations as well as longitudinal tracking of tumor shrinkage after the treatment are needed to validate theoretical predictions of this study.

The geometry of the simulation domain is greatly simplified in this study. The tumor is represented as a sphere rather than imported from image scans. The surrounding tissue block could be more realistic using the shape and size of the human breast and torso. The boundary condition prescribed on the tissue cylinder surface may be better described by an insulation boundary than a prescribed 37 °C boundary condition. Sensitivity studies are also needed to ensure that the tissue cylinder is sufficiently large to justify the prescribed boundary conditions. In addition, this study assumes homogeneity in consideration of nanoparticle distribution inside the tumor. In real applications, the

distribution of nanoparticles is often not uniform. Future work could analyze nanoparticle distribution using imaging techniques and evaluate how it affects the heating of the tumor and the resulting thermal damage. Future work could include development of a theoretical model using more realistic geometries and sizes of the tumor and breast to push the computational limits inherent with 3-D simulations.

5 Conclusions

We demonstrated selective laser ablation in a gold nanorod-deposited breast tumor model. A laser intensity of 24000 W/m^2 at the skin surface with a laser spot of 10 mm in diameter is needed to achieve a minimal temperature within the tumor at 47 °C. Results is used to design a heating protocol to inducing thermal damage to the entire tumor with a heating time of 916 s to completely damage the entire tumor. Although cold-water droplets are sprayed at the skin surface to protect skin and its surrounding tissue, it is found that collateral thermal damage to the healthy tissue near the tumor is inevitable. We conclude that theoretical simulation is demonstrated as a useful tool to evaluate temperature field during laser photothermal therapy and to design effective and safe heating protocols in clinical applications.

References

1. Hirsch, L.R., et al.: Nanoshell-mediated near-infrared thermal therapy of tumors under magnetic resonance guidance. Proc. Natl. Acad. Sci. U.S.A. **100**(23), 13549–13554 (2003)
2. El-Sayed, I.H., Huang, X., El-Sayed, M.A.: Selective laser photo-thermal therapy of epithelial carcinoma using anti-EGFR antibody conjugated gold nanoparticles. Cancer Lett. **239**(1), 129–135 (2006)
3. Jain, P.K., Lee, K.S., El-Sayed, I.H., El-Sayed, M.A.: Calculated absorption and scattering properties of gold nanoparticles of different size, shape, and composition: applications in biological imaging and biomedicine. J. Phys. Chem. B **110**(14), 7238–7248 (2006)
4. Skrabalak, S.E., Chen, J., Au, L., Lu, X., Li, X., Xia, Y.: Gold nanocages for biomedical applications. Adv. Mater. **19**, 3177–3184 (2007)
5. Khlebtsov, B., Zharov, V., Melnikov, A., Tuchin, V., Khlebtsov, N.: Optical amplification of photothermal therapy with gold nanoparticles and nanoclusters. Nanotechnology **17**, 5167–5179 (2006)
6. Manuchehrabadi, N., et al.: MicroCT imaging and in vivo temperature elevations in implanted prostatic tumors in laser photothermal therapy using gold nanorods. ASME J. Nanotechnol. Eng. Med. **3**, 021003(1–7) (2012)
7. Manuchehrabadi, N., et al.: Tumor shrinkage studies and histological analyses after laser photothermal therapy using gold nanorods. J. Biomed. Eng. Technol. **12**, 157–175 (2013)
8. Pennes, H.H.: Analysis of tissue and arterial blood temperature in the resting human forearm. J. Appl. Phys. **1**, 93–122 (1948)
9. Manuchehrabadi, N., Chen, Y., Lebrun, A., Ma, R., Zhu, L.: Computational simulation of temperature elevations in tumors using Monte Carlo method and comparison to experimental measurements in laser photothermal therapy. J. Biomech. Eng. **135**, 121007(1–11) (2013)
10. Manuchehrabadi, N., Zhu, L.: Development of a computational simulation tool to design a protocol for treating prostate tumours using transurethral laser photothermal therapy. Int. J. Hyperth. **30**(6), 349–361 (2014)

11. Mourant, J.R., Fuselier, T., Boyer, J., Johnson, T.M., Bigio, I.J.: Predictions and measurements of scattering and absorption over broad wavelength ranges in tissue phantoms. Appl. Opt. **36**(4), 949–957 (1997)